

1 **A new [indicator](#) on the impact of large-scale circulation on**
2 **wintertime particulate matter pollution over China**

3 Beixi Jia^{1,2}, Yuxuan Wang^{1,2,3}, Yu Yao¹ and Yuanyu Xie¹

4 ¹Ministry of Education Key Laboratory for Earth System Modeling, Center for Earth
5 System Science, Tsinghua University, Beijing, China.

6 ²Department of Marine Sciences, Texas A&M University at Galveston, Galveston,
7 TX, USA.

8 ³Department of Atmospheric Sciences, Texas A&M University, College Station,
9 TX, USA.

10

11 Correspondence to: Y. Wang, yxw@tsinghua.edu.cn

12

13

14 **Abstract:**

15 Extreme particulate matter (PM) air pollution of January 2013 in China was found to
16 be associated with an anomalous eastward extension of the Siberian High (SH). We
17 developed a Siberian High position index (SHPI), which depicts the mean
18 longitudinal position of the SH, as a new indicator of the large-scale circulation
19 pattern that controls wintertime air quality in China. This SHPI explains 58%
20 (correlation coefficient of 0.76) of the interannual variability of wintertime aerosol
21 optical depth (AOD) retrieved by MODIS over North China (NC) during 2001-2013.
22 By contrast, the intensity-based conventional Siberian High Index (SHI) shows

23 essentially no skill in predicting this AOD variability. On the monthly scale, some
24 high-AOD months for NC are accompanied with extremely high SHPIs; notably,
25 extreme PM pollution of January 2013 can be explained by the SHPI value exceeding
26 2.6 times the standard deviation of the 2001-2013 January mean. When the SH
27 extends eastward, thus higher SHPI, prevailing northwesterly winds over NC are
28 suppressed not only in the lower troposphere but also in the middle troposphere,
29 leading to reduced southward transport of pollution from NC to South China (SC).
30 The SHPI hence exhibits a significantly negative correlation of -0.82 with MODIS
31 AOD over SC during 2001-2013, although the robustness of this correlation depends
32 on that of satellite-derived AOD. The suppressed northwesterly winds during
33 high-SHPI winters also lead to increased relative humidity (RH) over NC. Both the
34 wind and RH changes are responsible for enhanced PM pollution over NC during the
35 high-SHPI winters.

36

37 **1. Introduction**

38 January 2013 saw persistent and severe haze outbreaks in China, with
39 monthly-mean fine particulate matter (PM_{2.5}) levels exceeding 130 $\mu\text{g m}^{-3}$ at 28 cities
40 in 16 provinces. Previous studies have identified certain features of meteorological
41 conditions during this month that are partly responsible for such extreme pollution.
42 An abnormal high at 500 hPa was found over east China which suggested a weakened
43 East Asian trough with suppressed vertical mixing (Zhang et al., 2014; Yang et al.,
44 2013). In the lower atmosphere, surface winds were much weaker during severe haze

45 episodes (Zhang et al., 2014; Y. S. Wang et al., 2014). The average height of planetary
46 boundary layer (PBL) over North China Plain was about 50% lower during the haze
47 episodes than that during non-episode days (Huang et al., 2014; L.T. Wang et al.,
48 2014). Ambient relative humidity (RH), an important meteorological parameter
49 affecting secondary aerosols formation and their hygroscopic growth (Sun et al., 2013;
50 Y. X. Wang et al., 2014), has also been reported to be significantly higher during the
51 haze periods (Huang et al., 2014; Y. S. Wang et al., 2014).

52 The aforementioned studies did not address the question whether extreme air
53 pollution of January 2013 over China is connected with the anomaly of large-scale
54 circulation patterns at a temporal scale broader than that of the episodic cases. The
55 East Asian monsoon is the most prominent feature of large-scale circulation patterns
56 over the Eurasia continent. While the summer monsoon has been shown to play a
57 significant role in regulating the interannual variation of air pollution over China (L.
58 Zhang et al., 2010, Zhu et al., 2012), few study has examined the wintertime
59 association between the variability of monsoon-related large-scale circulation patterns
60 and air pollution. As the most important large-scale circulation patterns in winter, the
61 Siberian High has a significant influence on winter climate in Northern Eurasia, East
62 Asia, and even the whole Northern Hemisphere (e.g., Cohen et al., 2001; Gong et al.,
63 2002; Chernokulsky et al., 2013). The sea level pressure difference between the
64 Siberian High over the Asian continent and the Aleutian Low over North Pacific
65 causes strong northwesterly winds along the east flank of the Siberian High and the
66 East Asian Coast, which characterizes the East Asian winter monsoon (Chang et al.,

67 2012). Wu et al. (2002) reported a significant positive correlation between the
68 intensity of the Siberian High and the East Asian winter monsoon on the interannual
69 to interdecadal time-scales. The variation of the Siberian High may have an impact on
70 wintertime air quality over east China, for example by ways of influencing large-scale
71 wind fields and local meteorological conditions which control pollutant transport and
72 transformation.

73 This study investigates the possible connections between wintertime $PM_{2.5}$ in
74 eastern China and large-scale circulations on the interannual scale during 2001-2013.
75 Because long-term in situ observations of surface $PM_{2.5}$ are not available in China, we
76 use satellite-derived aerosol optical depth (AOD) as a proxy to represent the
77 distribution and variability of atmospheric aerosols. The paper is organized as follows.
78 Section 2 describes the data used in the analysis. In Section 3, we analyze the
79 anomalous meteorological conditions of January 2013 and define our study regions.
80 Section 4 examines the relationship of the Siberian High and AOD over China, and
81 develops an index to represent Siberian High variability which is able to explain the
82 interannual variations of AOD. In Section 5, we discuss the robustness of the index
83 we develop and compare it with other existing meteorological indices that may
84 influence wintertime air quality in China.

85

86 **2. Data**

87 **2.1 Aerosol Optical Depth**

88 AOD products from satellites have been used to infer surface $PM_{2.5}$

89 concentrations at scales ranging from urban to regional and to global (Liu et al., 2007;
90 H. Zhang et al., 2009; Lee et al., 2011; Hu et al., 2014; Boys et al., 2014; van
91 Donkelaar et al. 2014; Xie et al., 2015). To circumvent data scarcity of longer-term in
92 situ surface measurement over China, here we used AOD retrieved from the Moderate
93 Resolution Imaging Spectroradiometer (MODIS) sensor aboard both NASA
94 EOS-Terra and Aqua satellite as the proxy data to represent the distribution and
95 variability of PM_{2.5} air quality. Terra and Aqua are both polar-orbiting satellites
96 launched in December 1999 and May 2002, respectively. They provide data every one
97 to two days since February 2000 (Terra) and July 2002 (Aqua). MODIS retrieves
98 aerosol properties in seven wavelengths from 0.47 to 2.13 μm and separate algorithms
99 are applied over land and ocean (Tanré et al., 1997; Remer et al., 2005; Levy et al.,
100 2007). To improve the retrieval over bright-reflecting source regions, the Deep Blue
101 AOD algorithm was developed using multiple narrow-band channels at near-UV
102 wavelengths (Hsu et al., 2004). Although the AOD uncertainty over land
103 ($\pm 0.05 \pm 0.2 \times \text{AOD}$) is higher than that over ocean ($\pm 0.03 \pm 0.05 \times \text{AOD}$) (Remer et al.,
104 2005; Chu et al., 2002), previous comparisons of MODIS AOD and ground-based
105 AOD measurements from AEROSOL ROBOTIC NETWORK (AERONET) sites over land
106 have shown tight correlations between the two, indicating that the MODIS AOD
107 product is capable of providing quantitative information on the spatial and temporal
108 variations of AOD over land (Levy et al., 2010; Prados et al., 2007).

109 Previous studies have indicated good correlations between the MODIS AOD
110 and surface PM_{2.5} concentrations over selected sites in China (Wang et al., 2003, Xie

111 et al., 2015). Here we used the MODIS level-3 monthly gridded AOD (550 nm) data
112 (Version 5.1) from December 2000 to February 2013 with a $1^\circ \times 1^\circ$ resolution. The
113 AOD values over bright surfaces were replaced by the Deep Blue aerosol retrieval
114 (550 nm) at the same grid.

115 To verify the robustness of our analysis using MODIS AOD, we also analyzed
116 level-3 monthly gridded AOD from Multi-angle Imaging SpectroRadiometer (MISR)
117 aboard of Terra. The MISR standard AOD products have a $0.5^\circ \times 0.5^\circ$ resolution at
118 558 nm for 2001-2013. MODIS has a large number of spectral bands, while MISR has
119 the multi-view-angle capabilities (Lyapustin et al., 2007).

120

121 **2.2 Reanalysis data**

122 The meteorological variables used to explore the mechanism behind the
123 variations of SH and AOD are obtained from National Centers for Environmental
124 Prediction (NCEP) reanalysis (Kalnay et al., 1996), including sea level pressure (SLP),
125 relative humidity (RH), geopotential heights, and winds. The NCEP/NCAR reanalysis
126 data provide a historical record of more than 50 years (Kistler et al., 2001) and are
127 available on the $2.5^\circ \times 2.5^\circ$ grid globally.

128 To verify the robustness of NCEP reanalysis in characterizing large-scale
129 circulation patterns, we also analyzed the reanalysis data from European Centre for
130 Medium-Range Weather Forecasts (ECMWF) Re-analysis Interim (ERA-Interim), the
131 latest global atmospheric reanalysis produced by ECMWF (Simons et al., 2007).
132 NCEP and ERA-Interim are the two widely used reanalysis products with relatively

133 long periods.

134

135 **3. Study domains**

136 Figure 1a shows the mean January SLP and 850 hPa wind fields during 2001-
137 2012 from NCEP. The Siberian High (SH) is a semi-permanent anticyclone high
138 pressure system centered over Mongolia and eastern Siberia (black rectangle in Figure
139 1a) that is formed by radiative cooling in winter. Driven by the pressure gradient
140 between the Siberian High and the Aleutian Low over northwest Pacific, the
141 prevailing winds over east China are northwesterly in winter. Figure 1b displays the
142 January 2013 SLP and the 850 hPa wind anomalies compared to the 2001-2012 mean.
143 The SLP was significantly lower over Mongolia in January 2013, indicating a
144 significantly weaker Siberian High and consequently a weaker East Asian winter
145 monsoon during this month. This anomalous SLP distribution of January 2013 is
146 associated with anomalous southerly winds in the lower atmosphere over east China
147 (Figure1b) and coincident with higher temperatures and RH (not shown), which all
148 present as favorable meteorological conditions for the buildup and recirculation of air
149 pollutants over this region (Sun et al., 2013; Zhang et al., 2014; Y.S. Wang et al.,
150 2014). Given the anomalously weak SH in January 2013, which was a
151 heavily-polluted month in China, we hypothesize that SH variability is a key indicator
152 of the variability in large-scale circulation patterns which control the variability of
153 wintertime PM pollutions over east China.

154 To test this hypothesis, we investigated if significant association exists in winter

155 between the SH variability and regional PM pollution over China on a longer-term
156 scale (2001-2013), using MODIS-derived AOD as an indicator of aerosols levels.
157 Figure 2a shows the 13-year mean winter AOD distribution over China and Figure 2b
158 displays the mean change of AOD from 2001-2006 to 2007-2013. North China (30°
159 $N-42^{\circ}N$, $115^{\circ}E-123^{\circ}E$; black rectangle in Figure 2b) is among the regions with
160 highest aerosol loadings and largest increases of AOD during the two averaging
161 periods. According to current emission inventories, the emissions of SO_2 , NO_x , and
162 NH_3 from North China accounts for 25%-35% of total emissions in China, and SO_2
163 emissions from North China have increased faster than those from other regions of
164 China (Lu et al., 2010; Y. Zhang et al., 2010; Q. Zhang et al., 2009). Therefore, North
165 China (NC) is defined as the source region of aerosols. According to the
166 climatological 850 hPa wind field (Figure 1a), the wintertime pollution outflow from
167 NC follows southeastwards pathways and is expected to influence air quality over
168 South China (SC), which is shown as the red rectangle in Figure 2b ($22^{\circ}N-30^{\circ}N$,
169 $110^{\circ}E-120^{\circ}E$). Here SC is defined as the domestic receptor region of NC aerosols in
170 winter.

171

172 **4. Development of the Siberian High position index and its association with AOD**

173 **4.1. Index development**

174 Figure 3 depicts the time series of winter AOD averaged over NC, showing a
175 significant increase in AOD from about 0.5 in 2001 to about 0.8 in 2013. A linear
176 regression of the time series gives a trend of $1.5\% \text{ year}^{-1}$ ($r=0.65$, $p<0.05$). Since the

177 meteorological variables and atmospheric circulation patterns are not expected to
178 drive such a large linear trend during this period, this AOD trend is mostly likely
179 caused by increasing anthropogenic emissions over this region (Lu et al., 2010, 2011;
180 Zhang et al., 2012; [Streets et al., 2009](#)). The departure of each winter's AOD from that
181 depicted by the linear trend is assumed to represent the influence of meteorology. The
182 years in which winter AOD lies above 30% of the residual confidence interval of the
183 linear trend line are referred to as the high-AOD winters (including 2001, 2003, 2007,
184 2008, 2013) and those below 30% of the residual confidence interval as the low-AOD
185 winters (including 2002, 2004, 2006, 2009, 2010, 2012). Since the high- or low-AOD
186 is defined relative to the trend line, the corresponding high- or low-AOD winters are
187 expected to be driven by the interannual variability of meteorology.

188 Mean meteorological conditions between the high- and low-AOD winters were
189 compiled and compared to identify any significant differences in large-scale
190 circulation patterns between them. The differences in winter-mean SLP and 850 hPa
191 wind fields are shown in Figure 4 (high-AOD winters minus low-AOD winters).
192 Surprisingly, Figure 4 does not reveal any significant decrease of SLP from low-AOD
193 to high-AOD winters over Mongolia where the climatological center of the Siberian
194 High locates (c.f. Figure 1a). Instead, significant changes of SLP are located over west
195 of Mongolia (negative differences) and over Japan (positive differences). The
196 high-AOD winters also have a stronger component of southeasterly winds at 850 hPa
197 over North China. This change of wind directions not only suppresses the
198 northwesterly flow that brings cleaner continental background air, but also reduces the

199 transport of pollution from NC to SC, both of which lead to higher pollution levels
200 over NC.

201 The index widely used in the literature to describe the SH variability is the
202 Siberian High intensity (SHI), defined as the mean SLP over northern Mongolia
203 between 80 °E -120 °E and 40 °N - 65 °N (black rectangle in Figure 1a and 4) (Jeong et
204 al., 2011; Hasanean et al., 2013). However, as shown by Figure 4, there is no
205 significant difference in SLP over northern Mongolia between the high- and
206 low-AOD winters, suggesting that this conventional index of SH may not be able to
207 explain the interannual variability of PM over North China. As an example, Figure 5
208 compares winter SLP and 850 hPa wind fields between 2003 (a high-AOD winter)
209 and 2004 (a low-AOD winter). While winter-mean AOD over NC was significantly
210 higher in 2003 (0.68) than that in 2004 (0.45), the SHI was almost the same between
211 the two winters. The noticeable difference, however, is that the high pressure isobars
212 in the 2003 winter extended further east over the continent than those in the 2004
213 winter. Through linear regression, we found a poor correlation between SHI and
214 detrended winter-mean AOD over NC (Figure 6a), with SHI explaining only 4% of
215 the AOD variance. [There is no significant \(\$p < 0.05\$ \) trend in SHI during 2001-2013.](#)

216 Figure 4 manifests the displacement of the high SLP center during the high-AOD
217 winters from northern Mongolia where the conventional SHI is defined. Figure 5
218 further illustrates that the main difference in SH between the two specific winters of
219 largely varying AODs lies in its spatial extension. Given this feature, we further
220 hypothesized that the position of the Siberian High is a more important factor than its

221 intensity in terms of affecting PM concentrations over NC. We thus proposed a
222 Siberian High position index (SHPI) as the weighted mean of the longitudes of all the
223 grids within the 1023 hPa isobar over the broad region of 60 °E -145 °E and 30 °N
224 -65 °N (black rectangle in Figure 5). The SHPI is defined by Equation 1:

$$225 \quad SHPI = \frac{\sum (P_i \times L_i)}{\sum P_i} \quad (1)$$

226 where L_i is the longitude of any eligible grid i within the 1023 hPa isobar and the
227 definition domain, and P_i is the SLP of the corresponding grid i . The unit of SHPI is
228 degree in longitude. Our definition of SHPI is similar to the longitude index of SH
229 defined by Hou et al. (2008), but differs with regards to the region over which SHPI is
230 calculated. They defined the index as the weighted mean longitudes of all the grids
231 within the 1023 hPa isobar which may extend westward to Europe and northward to
232 the Arctic. Our definition of SHPI limits the spatial domain over which the 1023 hPa
233 isobar is considered in the SHPI calculation because of our focus on East Asia and
234 particularly China (Figure 5). The 2001-2013 time series of winter SHPI is displayed
235 in Figure 6b (black line) and the wintertime mean SHPI during this period is 98.9 °E.
236 A larger SHPI indicates that the center of the Siberian High is located further east of
237 its normal position. Referring back to Figure 5, the 2003 winter has a significantly
238 higher value of SHPI (102.3 °E) than that of 2004 (SHPI = 96.3 °E); so does the AOD
239 over NC but not SHI (c.f. Figure 6a).

240 Figure 6b shows the time series of winter-mean SHPI and NC AOD from 2001 to
241 2013. They exhibit a positive correlation of 0.39, which is not significant due to the
242 confounding effect of the increasing trend in AOD. Since the focus here is on

243 variability, the AOD time series were detrended by removing any significant linear
244 trend (detrended AOD) and the SHPI time series were normalized by their
245 climatological mean and standard deviation. As shown in Figure 6c, the detrended NC
246 AOD and normalized SHPI display a strong correlation of 0.76 ($p < 0.01$), which
247 means that the position-based SHPI captures 58% of the interannual variance in
248 winter AOD over NC. This indicates that on the interannual scale, winter AOD over
249 NC can be better explained by SHPI, an index of the SH position, than the
250 conventional SHI, an index of the SH intensity. According to Hou et al. (2008), the
251 longitude index and intensity index of the SH may not be significantly correlated. In
252 support of this point, we found the SHI and SHPI have a weak correlation of only
253 -0.32 during the study period (Figure S1).

254 Figure 6d displays the time series of normalized SHPI and detrended NC AOD on
255 the monthly scale. The corresponding raw data prior to the detrending and
256 normalization are provided in Figure S2. Here the normalization of SHPI is conducted
257 separately for November, December, and January to retain its intraseasonal variability.
258 At the monthly scale, the correlation between normalized SHPI and detrended NC
259 AOD is also significant at 0.45 ($p < 0.01$). Some extremely high values of monthly
260 AOD over NC show clear associations with higher values of SHPI. Taking January
261 2013 as an example, which has the highest AOD over NC among all the 39 winter
262 months studied here, the SHPI of that month is also the highest (106.5 σ), lying 2.6
263 times the standard deviation away from the 2001-2013 January mean (99.8 σ). This
264 association indicates that the anomalous feature of the Siberian High in January 2013

265 was not only the weakening of its strength (c.f. Figure 1b) but also its more eastward
266 extension, the latter being the primary factor contributing to high PM levels over NC.
267 Another example is February 2011. Both AOD and SHPI of that month are among the
268 highest values of the study period (Figure 6d and S2). We thus conclude that the SHPI
269 indicator of the SH variability is able to explain extremely high PM pollution over NC
270 on the monthly scale.

271

272 **4.2. Mechanism**

273 To understand the mechanistic connection between SHPI and winter AOD over
274 NC, we examine in this section how the SHPI variability is linked with the change of
275 large-scale circulation patterns using the NCEP reanalysis data which span 30 years
276 (1982-2011). The years with extremely high SHPI (beyond one standard deviation of
277 the mean) in winter are defined to be high-SHPI years and those below one standard
278 deviation of the mean as low-SHPI years. Figure 7a displays the climatological
279 distribution of 850 hPa wind fields during 1982-2011. The northwesterly winds larger
280 than 5 m s^{-1} over North China and Japan indicate the strong influence of the Siberian
281 High and East Asian winter monsoon. The area covered by the prevailing
282 northwesterly winds and the mean speed of those winds exhibit interannual variability
283 that correlates with SHPI to some extent. For example, the winter of 1990 has the
284 highest SHPI ($105.9 \text{ \textcircled{E}}$) during the 30-year study period and that of 2004 has the
285 lowest SHPI ($96.3 \text{ \textcircled{E}}$). As shown in Figure S3, the area covered by northwesterly
286 winds larger than 5 m s^{-1} is smaller in 1990 than that in 2004, and the average wind

287 speed over that area is also smaller in 1990. On average, 850 hPa wind speeds over
288 NC are about 0.5 m s^{-1} to 1 m s^{-1} lower during the high-SHPI winters than during the
289 low-SHPI years (Figure 7b). Table 1 summarizes wintertime-mean zonal and
290 meridional wind speeds over NC at different vertical levels for the 30-year average,
291 high-SHPI average, and low-SHPI average. In the high-SHPI winters, both zonal and
292 meridional wind speeds are lower not only at 850 hPa but also at the upper levels.
293 Lower wind speeds are conducive for pollution accumulation over the source region,
294 which partly contributes to higher AOD in the high-SHPI winters. To further illustrate
295 the connections between SHPI and wind changes, Figure 7c depicts the spatial
296 distribution of correlation coefficients between SHPI and surface RH from 1982 to
297 2011. SHPI shows a significant positive correlation with RH over NC, indicating
298 enhanced water vapor convergence over NC in the high-SHPI winters. This positive
299 correlation arises because weaker northerly winds lead to reduced transport of dry air
300 masses from the cold Siberian landmass, compensated by enhanced transport of moist
301 air masses through the anomalous southerly winds. Higher RH during the high-SHPI
302 winters leads to higher mass concentrations and extinction of aerosols as a result of
303 hygroscopic growth of aerosol species (Mu et al., 2014; Tai et al., 2010). Although
304 higher SHPI is always associated with lower northwesterly wind and higher RH over
305 NC, local wind speed or RH itself is not an indicator as good as SHPI in explaining
306 the interannual variation of NC AOD. One explanation is that SHPI represents the
307 combined effects of large-scale circulation change on local meteorological conditions.
308 In addition, systematic errors have been found for lower-level wind fields from NCEP

309 reanalysis (Shi et al., 2006).

310 To verify the above analysis of the mechanism, we tested the utility of SLP over
311 Japan (SLPJ, defined over 130 °E-145 °E and 40 °N-50 °N) as an alternative indicator
312 of the large-scale circulation in explaining the interannual variations of AOD over NC.
313 The reason why the SLPJ is used for comparison is because the high-AOD winters
314 also feature significant positive changes of SLP over (c.f. Figure 4). The time series of
315 SLPJ is shown in Figure S4. SLPJ shows a positive correlation with NC AOD and
316 explains 38% of the variance in detrended NC AOD (Figure S4a). By comparison,
317 SHPI explains 58% of the variance of detrended NC AOD. SLPJ also correlates well
318 with SHPI (Figure S4b), which indicates that in the high-SHPI years the eastward
319 extension of the SH leads to an increase of SLP over Japan and as a result SLPJ is not
320 independent from SHPI. The anomalously high SLP over Japan influences the PM
321 level over NC by reducing the prevailing northwesterly winds and increasing RH over
322 NC, which is consistent with the mechanism provided above.

323 To summarize, the SHPI indicator developed here is able to capture the
324 interannual variations of winter-mean and monthly-mean NC AOD to a large extent.
325 Comparing to the climatology, 850 hPa wind speeds over NC during the high-SHPI
326 years are suppressed by 13% and the surface relative humidity is enhanced by 12% as
327 a result of the eastward extension of the SH. Since the suppressed wind speed is
328 unfavorable for the [dispersion](#) of air pollution and higher surface relative humidity
329 enhances secondary aerosol formation and hygroscopic growth, both factors lead to
330 higher PM levels over NC in the high-SHPI years.

331

332 **4.3. AOD variability in South China**

333 Our above analysis suggests that the suppression of prevailing northwesterly
334 winds and the enhancement of surface RH are the key meteorological features during
335 the high-SHPI winters. The implication of such conditions for wintertime PM over SC,
336 the domestic receptor region of wintertime NC outflow, is not straightforward. On one
337 hand, suppressed northwesterly winds are unfavorable meteorological conditions for
338 the export of pollution from NC, which may lead to reduced PM levels over SC. On
339 the other hand, the Siberian High variability is expected to have an influence on local
340 meteorological conditions over SC. In this section, we examine the extent to which
341 the SHPI indicator developed in the previous section can explain the interannual
342 variability of AOD over SC.

343 Figure 8 displays the time series of winter mean AOD over SC from MODIS. The
344 multi-year mean AOD over SC is about 0.4, with a positive but not significant trend
345 of increase of $0.13\% \text{ year}^{-1}$. The two highest AOD winters for SC are 2004 (0.46) and
346 2008 (0.48), both corresponding to the lowest SHPI. The overall correlation between
347 SC AOD and normalized SHPI is -0.82, suggesting that SHPI explains 67% of the
348 variance in SC AOD. In the high-SHPI winters, the meridional wind speed over NC is
349 reduced by 17%, 16% and 19% at 850 hPa, 700 hPa, and 500 hPa, respectively,
350 compared to the low-SHPI winters (Table 1). The suppressed northerly winds over
351 NC lead to the direct effect of reduced southward transport of pollution from NC to
352 SC, resulting in lower AOD over SC during the high-SHPI winters. Meanwhile, the

353 850 hPa wind speeds over SC does not show a significant difference between the
354 high-SHPI and low-SHPI winters (Figure 7b). Although there is a 7.5% enhancement
355 of surface relative humidity over SC during the high-SHPI years (Figure 7c), the
356 overall significantly negative correlation between SC AOD and SHPI indicate that the
357 suppressed pollution transport from NC to SC is the dominant factor to explain the
358 influence of SHPI on AOD over SC.

359

360 **5. Discussion**

361 To test the robustness of the relationship between AOD and SHPI developed
362 above using MODIS AOD and NCEP reanalysis, we conducted the same analysis
363 using AOD derived from MISR (MISR AOD) and SHPI derived from the
364 ERA-Interim reanalysis (ERA SHPI). Table 2 compares the correlation coefficients
365 derived using the different datasets. Significant positive correlations are consistently
366 found between the SHPI and AOD over NC, regardless of the data sources from
367 which the SHPI and AOD are derived. For example, the ERA SHPI has a correlation
368 of 0.65 with MISR AOD over NC, compared to that of 0.76 between NCEP SHPI and
369 MODIS AOD. This indicates the robustness of the SHPI indicator developed here
370 with regard to explaining the interannual variability of AOD over NC. However, the
371 correlation between SHPI and AOD over SC displays a dependence on the data source.
372 The ERA SHPI has a similarly strong negative correlation with MODIS AOD over SC
373 as the NCEP SHPI does, but neither NCEP SHPI nor ERA SHPI correlates well with
374 MISR AOD over this region. This discrepancy can be partly explained by the

375 inconsistency in the interannual variability of AOD between MODIS and MISR over
376 SC. As shown in Figure S5a, the correlation coefficient between the two AOD time
377 series is only 0.07 over SC during 2001-2013, although neither shows a significant
378 increasing trend. By comparison, the AOD time series from MODIS and MISR show
379 a strong correlation of 0.7 over NC (Figure S5b). Since SC has more cloud coverage
380 than NC (Li et al., 2004), the inconsistency between MODIS and MISR over SC may
381 lie in the different cloud-screening algorithms between MODIS and MISR. In
382 addition, MISR has a lower sampling frequency than MODIS which may also lead to
383 the inconsistency (Y. Zhang et al., 2010). Therefore, our conclusion on the association
384 of SHPI with AOD variability over SC may require verification by later studies.

385 In addition to the conventional SHI, the number of cold air surges has been used
386 as an indicator of the strength of the SH in winter. A cold air surge is an influx of
387 unusually cold continental air from the Arctic Ocean and Siberia into the middle or
388 lower latitudes, and it is the main disastrous weather influencing China in the winter
389 half-year. Niu et al. (2010) reported that the number of cold air surges decreased
390 significantly from 1976 to 2007, which coincided with the increasing frequency of
391 wintertime fog over eastern-central China. Varieties of definitions have been used for
392 cold air surges, such as changes in surface temperature, surface pressure, and wind
393 speed (Wang, 2006). The definition of cold air surges we used is as follows. We took
394 8 sites in North China (Jiuquan, Lanzhou, Beijing, Shenyang, Changchun, Haerbin,
395 Xi'an, Ji'nan) and 7 sites in South China (Nanjing, Hankou, Chengdu, Changsha,
396 Guiyang, Fuzhou, Guangzhou). If the 15-site mean daily temperature keeps

397 decreasing for three days and the overall magnitude of this temperature decrease is
398 larger than 5°C, it is considered as a cold air surge. The number of cold air surges per
399 winter during 2001-2013 is shown in Figure S6, which explains less than 15% of the
400 variance in the interannual variability of AOD over NC and SC. Thus, SHPI fares
401 better than the number of cold air surges in explaining the interannual variability of
402 AODs over different regions of China.

403 To summarize, through analyzing the anomalous meteorological conditions
404 during January 2013, we have revealed not only the weakening of the strength of the
405 Siberian High over Mongolia, but also its more eastward extension, the latter being
406 the key factor contributing to high PM levels over NC. Thus, the Siberian High
407 Position Index (SHPI) depicting the mean longitudinal position of the Siberian High is
408 developed, and this index captures 58% of the interannual variance in winter AOD
409 over NC during 2001-2013. The SHPI is able to indicate the occurrence of high PM
410 pollution levels over NC on the monthly scale; notably, the extreme PM pollution of
411 January 2013 over NC is associated with an extremely high value of SHPI (above 2.6
412 times standard deviation of the 2001-2013 mean). Mechanistic analysis indicates that
413 high SHPI is often associated with suppressed prevailing northwesterly winds and
414 higher relative humidity over NC, both of which are favorable for secondary
415 formation and accumulation of PM over NC. The suppressed prevailing winds over
416 NC also weaken the southward transport of pollution to SC, resulting in lower PM
417 levels over SC. The positive correlations between NC AOD and SHPI also exist
418 among different datasets we tested, including NCEP and ERA-Interim for SHPI and

419 MODIS and MISR for AOD. However, the negative correlation between AOD and
420 SHPI over SC is significant only using AOD derived from MODIS and thus needs to
421 be further confirmed.

422

423 **Acknowledgement:** This research was supported by the National Key Basic Research
424 Program of China (2013CB956603 and 2014CB441302) and the CAS Strategic
425 Priority Research Program (Grant No. XDA05100403). We thank Lu Shen for helpful
426 discussion.

427

428 **References**

429 Boys, B. L., Martin, R. V., van Donkelaar, A., MacDonell, R. J., Hsu, N. C., Cooper, M. J.,
430 Yantosca, R. M., Lu, Z., Streets, D. G., Zhang, Q., and Wang, S. W.: Fifteen-year global time
431 series of satellite-derived fine particulate matter, *Environ. Sci. Technol.*, 48, 11109-11118,
432 doi:10.1021/es502113p, 2014.

433 Chang, C. P. and Lu, M. M.: Intraseasonal predictability of Siberian High and East Asian winter
434 monsoon and its interdecadal variability, *J. Climate*, 25, 1773-1778, doi:10.1175/JCLI-
435 D-11-00500.1, 2012.

436 Chernokulsky, A., Mokhov, I. I., and Nikitina, N.: Winter cloudiness variability over northern
437 Eurasia related to the Siberian High during 1966-2010, *Environ. Res. Lett.*, 8, 045012,
438 doi:10.1088/1748-9326/8/4/045012, 2013.

439 Chu, D. A., Kaufman, Y. J., Ichoku, C., Remer, L. A., Tanré D., and Holben, B. N.: Validation of
440 MODIS aerosol optical depth retrieval over land, *Geophys. Res. Lett.*, 29, 1617, doi:

441 10.1029/2001GL013205, 2002.

442 Cohen, J., Saito, K., and Entekhabi, D.: The role of the Siberian High in Northern Hemisphere
443 climate variability, *Geophys. Res. Lett.*, 28, 299-302, doi:10.1029/2000GL011927, 2001.

444 Gong, D. Y. and Ho, C. H.: The Siberian High and climate change over middle to high latitude
445 Asia, *Theor. Appl. Climatol.*, 72, 1-9, doi:10.1007/s007040200008, 2002.

446 Hasanean, H. M., Almazroui, M., Jones, P. D., and Alamoudi, A. A.: Siberian high variability and
447 its teleconnections with tropical circulations and surface air temperature over Saudi Arabia,
448 *Clim. Dynam.*, 41, 2003-2018, doi:10.1007/s00382-012-1657-9, 2013.

449 Hou, Y. H., Yang, X. Q., Li, G., and Wang, Q.: Four indexes and their change rates Siberian High,
450 *Journal of Nanjing Institute of Meteorology*, 31, 326-330, 2008 (in Chinese).

451 Hsu, N. C., Tsay, S. C., King, M. D., and Herman, J. R.: Aerosol properties over bright-reflecting
452 source regions, *IEEE T. Geosci. Remote*, 42, 557-569, doi:10.1109/TGRS.2004.824067, 2004.

453 Hu, X., Waller, L. A., Lyapustin, A., Wang, Y., and Liu, Y.: 10-year spatial and temporal trends
454 of PM_{2.5} concentrations in the southeastern US estimated using high-resolution satellite data,
455 *Atmos. Chem. Phys.*, 14, 6301-6314, doi:10.5194/acp-14-6301-2014, 2014.

456 Huang, K., Zhuang, G., Wang, Q., Fu, J. S., Lin, Y., Liu, T., Han, L., and Deng, C.: Extreme haze
457 pollution in Beijing during January 2013: chemical characteristics, formation mechanism and
458 role of fog processing, *Atmos. Chem. Phys. Discuss.*, 14, 7517-7556, doi: 10.5194/
459 acpd-14-7517-2014, 2014.

460 Jeong, J. H., Ou, T., Linderholm, H. W., Kim, B. M., Kim, S.-J., Kug, J. S., and Chen, D.: Recent
461 recovery of the Siberian High intensity, *J. Geophys. Res. -Atmos.*, 116, D23102, doi:
462 10.1029/2011JD015904, 2011.

463 Kalnay, E., Kanamitsu, M., Kistler, R., Collins, W., Deaven, D., Gandin, L., Iredell, M., Saha, S.,
464 White, G., Woollen, J., Zhu, Y., Leetmaa, A., Reynolds, R., Chelliah, M., Ebisuzaki, W.,
465 Higgins, W., Janowiak, J., Mo, K. C., Ropelewski, C., Wang, J., Jenne, R., and Joseph, D.: The
466 NCEP/NCAR 40-year reanalysis project, *B. Am. Meteorol. Soc.*, *77*, 437-473, 1996.

467 Kistler, R., Collins, W., Saha, S., White, G., Woollen, J., Kalnay, E., Chelliah, M., Ebisuzaki, W.,
468 Kanamitsu, M., Kousky, V., Dool, H., Jenne, R., and Fiorino, M.: The NCEP-NCAR 50-year
469 reanalysis: monthly means CD-ROM and documentation, *B. Am. Meteorol. Soc.*, *82*, 247-267,
470 2001.

471 Lee, H. J., Liu, Y., Coull, B. A., Schwartz, J., and Koutrakis, P.: A novel calibration approach of
472 MODIS AOD data to predict PM_{2.5} concentrations, *Atmos. Chem. Phys.*, *11*, 7991-8002,
473 doi:10.5194/acp-11-7991-2011, 2011.

474 Levy, R. C., Remer, L. A., Mattoo, S., Vermote, E. F., and Kaufman, Y. J.: Second-generation
475 operational algorithm: retrieval of aerosol properties over land from inversion of Moderate
476 Resolution Imaging Spectroradiometer spectral reflectance, *J. Geophys. Res. -Atmos.*,
477 112(D13211), doi:10.1029/2006JD007811, 2007.

478 Levy, R. C., Remer, L. A., Kleidman, R. G., Mattoo, S., Ichoku, C., Kahn, R., and Eck, T. F.:
479 Global evaluation of the Collection 5 MODIS dark-target aerosol products over land, *Atmos.*
480 *Chem. Phys.*, *10*, 10399-10420, doi:10.5194/acp-10-10399-2010, 2010.

481 [Li, Y., Yu, R. C., Xu, Y. P., and Zhang, X. H.: Spatial Distribution and Seasonal Variation of Cloud](#)
482 [over China Based on ISCCP Data and Surface Observations, *J. Meteorol. Soc. Jpn.*, *82*,761-773,](#)
483 [doi: 10.2151/jmsj.2004.761, 2004.](#)

484 Liu, Y., Franklin, M., Kahn, R., and Koutrakis, P.: Using aerosol optical thickness to predict

485 ground-level PM_{2.5} concentrations in the St. Louis area: a comparison between MISR and
486 MODIS, *Remote Sens. Environ.*, 107, 33-44, doi:10.1016/j.rse.2006.05.022, 2007.

487 Lu, Z., Streets, D. G., Zhang, Q., Wang, S., Carmichael, G. R., Cheng, Y. F., Wei, C., Chin, M.,
488 Diehl, T., and Tan, Q.: Sulfur dioxide emissions in China and sulfur trends in East Asia since
489 2000, *Atmos. Chem. Phys.*, 10, 6311-6331, doi:10.5194/acp-10-6311-2010, 2010.

490 Lu, Z., Zhang, Q., and Streets, D. G.: Sulfur dioxide and primary carbonaceous aerosol emissions
491 in China and India, 1996-2010, *Atmos. Chem. Phys.*, 11, 9839-9864, doi:10.5194/acp-
492 11-9839-2011, 2011.

493 Lyapustin, A., Wang, Y., Kahn, R., Xiong, J., Ignatov, A., Wolfe, R., Wu, A., Holben, B., and
494 Bruegge, C.: Analysis of MODIS-MISR calibration differences using surface albedo around
495 AERONET sites and cloud reflectance, *Remote Sens. Environ.*, 107, 12-21, doi:
496 10.1016/j.rse.2006.09.028, 2007.

497 Mu, Q. and Liao, H.: Simulation of the interannual variations of aerosols in China: role of
498 variations in meteorological parameters, *Atmos. Chem. Phys.*, 14, 9597-9612, doi:10.5194/acp-
499 14-9597-2014, 2014.

500 Niu, F. Z., Li, Q., Li, C., Kwon-Ho, L., and Zhang, M. Y.: Increase of wintertime fog in China:
501 potential impacts of weakening of the eastern Asian monsoon circulation and increasing
502 aerosol loading, *J. Geophys. Res. -Atmos.*, 115, D00k20, doi:10.1029/2009JD013484, 2010.

503 Prados, A. I., Kondragunta, S., Ciren, P., and Knapp, K. R.: GOES Aerosol/Smoke Product
504 (GASP) over North America: comparisons to AERONET and MODIS observations, *J.*
505 *Geophys. Res. -Atmos.*, 112, D15201, doi:10.1029/2006jd007968, 2007.

506 Remer, L. A., Kaufman, Y. J., Tanré D., Mattoo, S., Chu, D. A., Martins, J. V., Li, R.-R., Ichoku,

507 C., Levy, R. C., Kleidman, R. G., Eck, T. F., Vermote, E., and Holben, B. N.: The MODIS
508 aerosol algorithm, products, and validation, *J. Atmos. Sci.*, 62, 947-973,
509 doi:10.1175/JAS3385.1, 2005.

510 Shi, X. H., Xu, X., and Xie, L.: Reliability analysis of anomalies of NCEP/NCAR reanalysis wind
511 speed and surface temperature in climate change research in China, *J. Meteor. Res.*, 6, 709-722,
512 2006 (in Chinese).

513 Simmons, A., Uppala, S., Dee, D., and Kobayashi, S.: ERA-Interim: new ECMWF reanalysis
514 products from 1989 onwards, *ECMWF Newsletter*, 110, 25-35, 2007.

515 Streets, D. G., Yan, F., Chin, M., Diehl, T., Mahowald, N., Schultz, M., Wild, M., Wu, Y., and Yu,
516 C.: Anthropogenic and natural contributions to regional trends in aerosol optical depth,
517 1980-2006, *J. Geophys. Res.*, 114, D00D18, doi: 10.1029/2008JD011624, 2009.

518 Sun, Y., Wang, Z., Fu, P., Jiang, Q., Yang, T., Li, J., and Ge, X.: The impact of relative humidity
519 on aerosol composition and evolution processes during wintertime in Beijing, China, *Atmos.*
520 *Environ.*, 77, 927-934, doi:10.1016/j.atmosenv.2013.06.019, 2013.

521 Tai, A. P. K., Mickley, L. J., and Jacob, D. J.: Correlations between fine particulate matter (PM_{2.5})
522 and meteorological variables in the United States: implications for the sensitivity of PM_{2.5} to
523 climate change, *Atmos. Environ.*, 44, 3976-3984, doi:10.1016/j.atmosenv.2010.06.060, 2010.

524 Tanré D., Kaufman, Y. J., Herman, M., and Mattoo, S.: Remote sensing of aerosol properties over
525 oceans using the MODIS/EOS spectral radiances, *J. Geophys. Res. -Atmos.*, 102, 16971, doi:
526 10.1029/96jd03437, 1997.

527 van Donkelaar, A. A., Martin, R. V., Brauer, M., and Boys, B. L.: Use of satellite observations for
528 long-term exposure assessment of global concentrations of fine particulate matter, *Environ.*

529 Health Persp., 123, 135-143, doi:10.1289/ehp.1408646, 2014.

530 Wang, J. and Christopher, S. A.: Intercomparison between satellite-derived aerosol optical
531 thickness and PM_{2.5} mass: implications for air quality studies, *Geophys. Res. Lett.*, 30, 2095,
532 doi: 10.1029/2003gl018174, 2003.

533 Wang, B.: *The Asian Monsoon*, 189 pp., Springer, New York, 2006.

534 Wang, L. T., Wei, Z., Yang, J., Zhang, Y., Zhang, F. F., Su, J., Meng, C. C., and Zhang, Q.: The
535 2013 severe haze over southern Hebei, China: model evaluation, source apportionment, and
536 policy implications, *Atmos. Chem. Phys.*, 14, 3151-3173, doi: 10.5194/acp-14-3151-2014,
537 2014.

538 Wang, Y. X., Zhang, Q. Q., Jiang, J., Zhou, W., Wang, B., He, K., Duan, F., Zhang, Q., Philip, S.,
539 and Xie, Y.: Enhanced sulfate formation during China's severe winter haze episode in January
540 2013 missing from current models, *J. Geophys. Res. -Atmos.*, 119, 10425-10440, doi:
541 10.1002/2013JD021426, 2014.

542 Wang, Y. S., Yao, L., Wang, L., Liu, Z., Ji, D., Tang, G., Zhang, J., Sun, Y., Hu, B., and Xin, J.:
543 Mechanism for the formation of the January 2013 heavy haze pollution episode over central
544 and eastern China, *Sci. China Ser. D*, 57, 14-25, doi: 10.1007/s11430-013-4773-4, 2014.

545 Wu, B. and Wang, J.: Winter Arctic oscillation, Siberian High and East Asian winter monsoon,
546 *Geophys. Res. Lett.*, 29, 1897, doi: 10.1029/2002GL015373, 2002.

547 Xie, Y.Y., Wang, Y., Zhang, K., Dong, W., Lv, B., and Bai, Y.: Daily estimation of ground-level
548 PM_{2.5} concentrations over Beijing using 3 km resolution MODIS AOD, *Environ. Sci. Technol.*
549 (Just accepted manuscript), doi: 10.1021/acs.est.5b01413, 2015.

550 Yang, K., Dickerson, R. R., Carn, S. A., Ge, C., and Wang, J.: First observations of SO₂ from the

551 satellite Suomi NPP OMPS: widespread air pollution events over China, *Geophys. Res. Lett.*,
552 40, 4957-4962, doi: 10.1002/grl.50952, 2013.

553 Zhang, H., Hoff, R. M., and Engel-Cox, J. A.: The relation between Moderate Resolution Imaging
554 Spectroradiometer (MODIS) aerosol optical depth and PM_{2.5} over the United States: a
555 geographical comparison by U.S. Environmental Protection Agency regions, *JAPCA J. Air*
556 *Waste Ma.*, 59, 1358-1369, doi:10.3155/1047-3289.59.11.1358, 2009.

557 Zhang, Q., Streets, D. G., Carmichael, G. R., He, K. B., Huo, H., Kannari, A., Klimont, Z., Park, I.
558 S., Reddy, S., Fu, J. S., Chen, D., Duan, L., Lei, Y., Wang, L. T., and Yao, Z. L.: Asian
559 emissions in 2006 for the NASA INTEX-B mission, *Atmos. Chem. Phys.*, 9, 5131-5153,
560 doi:10.5194/acp-9-5131-2009, 2009.

561 Zhang, Y. and Sun, Z.: Comparisons of MODIS and MISR aerosol optical thickness over
562 eastcentral China, *Journal of the Meteorological Sciences*, 30, 48-54, 2010 (in Chinese).

563 Zhang, Y., Dore, A. J., Ma, L., Liu, X. J., Ma, W. Q., Cape, J. N., and Zhang, F. S.: Agricultural
564 ammonia emissions inventory and spatial distribution in the North China Plain, *Environ. Pollut.*,
565 158, 490-501, doi:10.1016/j.envpol.2009.08.033, 2010.

566 Zhang, L., Liao, H., and Li, J.: Impacts of Asian summer monsoon on seasonal and interannual
567 variations of aerosols over eastern China, *J. Geophys. Res.*, 115, D00K05,
568 doi:10.1029/2009JD012299, 2010.

569 Zhang, Q., Geng, G. N., Wang, S. W., Richter, A., and He, K. B.: Satellite remote sensing of
570 changes in NO_x emissions over China during 1996-2010, *Chinese Sci. Bull.*, 57, 2857-2864,
571 doi:10.1007/s11434-012-5015-4, 2012.

572 Zhang, R. H., Li, Q., and Zhang, R. N.: Meteorological conditions for the persistent severe fog and

573 haze event over eastern China in January 2013, *Sci. China Ser. D*, 57, 26-35,

574 doi:10.1007/s11430-013-4774-3, 2014.

575 Zhu, J., Liao, H., and Li, J.: Increases in aerosol concentrations over eastern China due to the

576 decadal-scale weakening of the East Asian summer monsoon, *Geophys. Res. Lett.*, 39, L09809,

577 doi:10.1029/2012GL051428, 2012.

578

579 **Tables**

580 Table 1. Mean zonal (U) and meridional (V) wind speeds over NC at different
 581 pressure levels (850 hPa, 700 hPa, and 500 hPa) during all winters (1982-2011), the
 582 high-SHPI winters, and the low-SHPI winters. The high- and low-SHPI winters are
 583 defined as the winters with the SHPI value lying outside of one standard deviation
 584 above or below the mean, respectively. Unit: m s^{-1}

	850hPa		700hPa		500hPa	
	U	V	U	V	U	V
All winters (1982-2011)	4.18	-3.06	10.94	-3.22	23.30	-3.17
High-SHPI winters	3.83	-2.67	10.39	-2.66	21.58	-2.33
Low-SHPI winters	4.26	-3.18	11.23	-3.17	24.24	-2.94

585

586 Table 2. Correlation coefficients between SHPI and AOD derived from different
 587 datasets: NCEP and ERA-Interim for SHPI, and MODIS and MISR for AOD.

	North China (NC) AOD		South China (SC) AOD	
	MODIS	MISR	MODIS	MISR
NCEP SHPI	0.76	0.67	-0.82	0.03
ERA SHPI	0.79	0.65	-0.74	-0.09

588

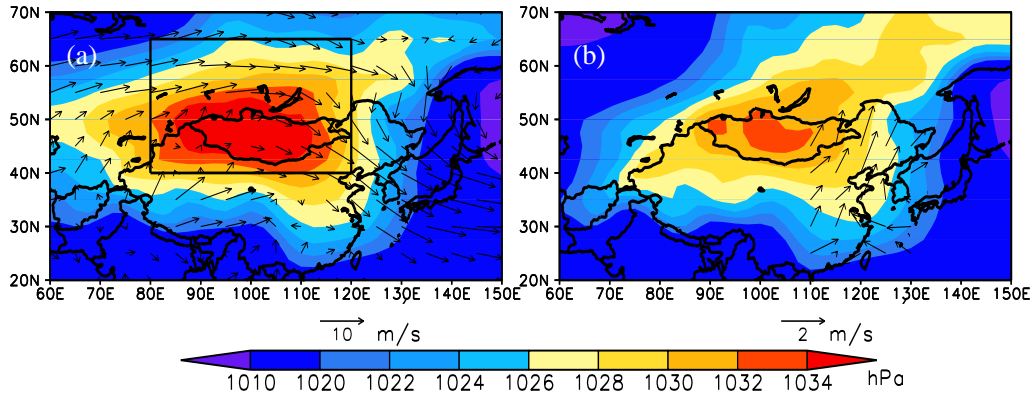
589

590

591

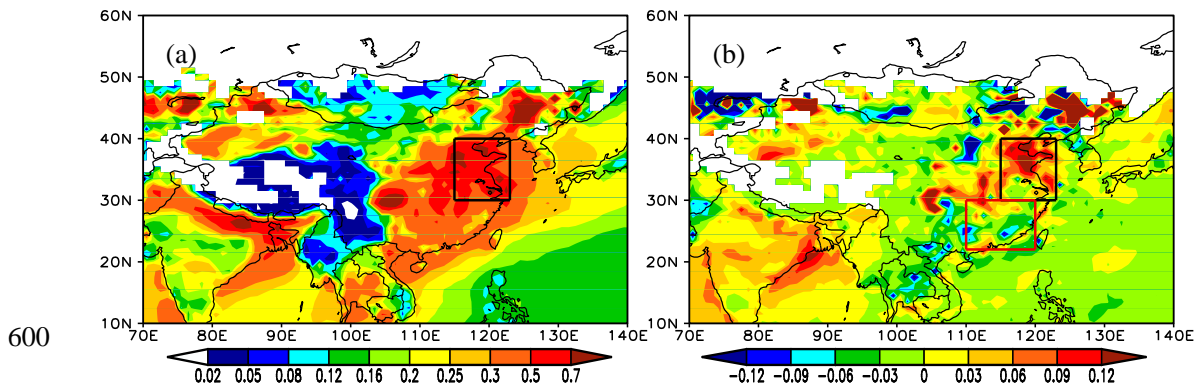
592

593 **Figures**



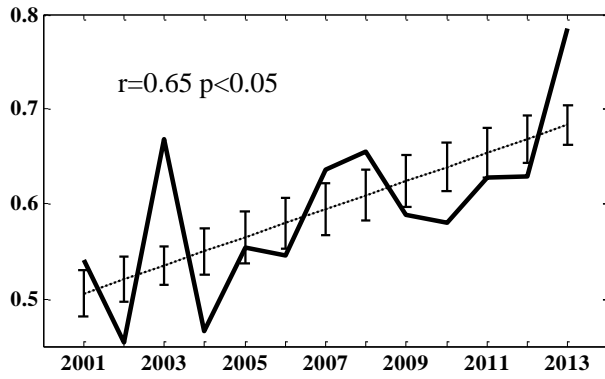
594

595 Figure 1. (a) Multi-year (2001-2012) mean January SLP (shaded) and 850 hPa wind
596 fields (vectors); (b) January 2013 SLP (shaded) and the anomalies 850 hPa wind
597 fields (vectors); the black rectangle outlines the region used in the definition of
598 conventional Siberian High intensity. The length of the wind vectors indicates wind
599 speed (m s^{-1}).



600

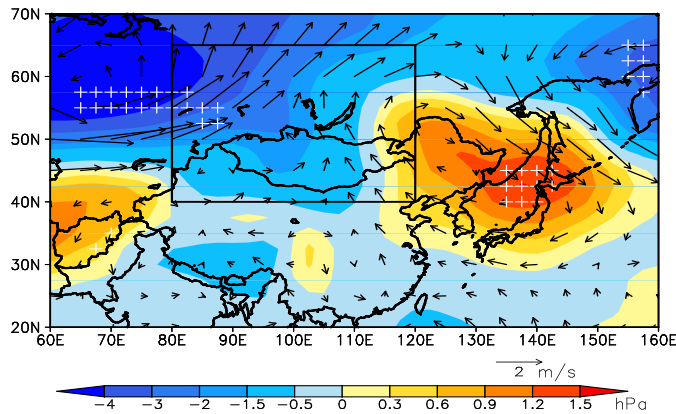
601 Figure 2. (a) Multi-year mean winter AOD from 2001-2013; (b) the change of winter
602 mean AOD between 2007-2013 and 2001-2006 (2007-2013 minus 2001-2006). The
603 black rectangle outlines North China (NC); the red rectangle outlines South China
604 (SC).



605

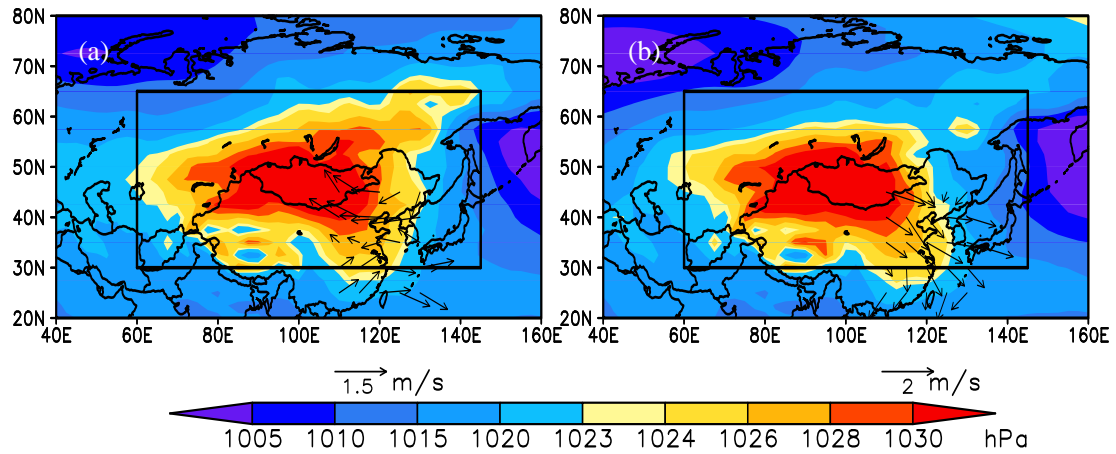
606 Figure 3. Time series of winter mean AOD over North China (solid thick line) and the
 607 fitted linear regression line (dotted thin line). The insert shows the correlation
 608 coefficient (r) and significance of the linear regression. The vertical thin line indicates
 609 the residual confidence interval of the linear regression slope ($\alpha=0.7$).

610



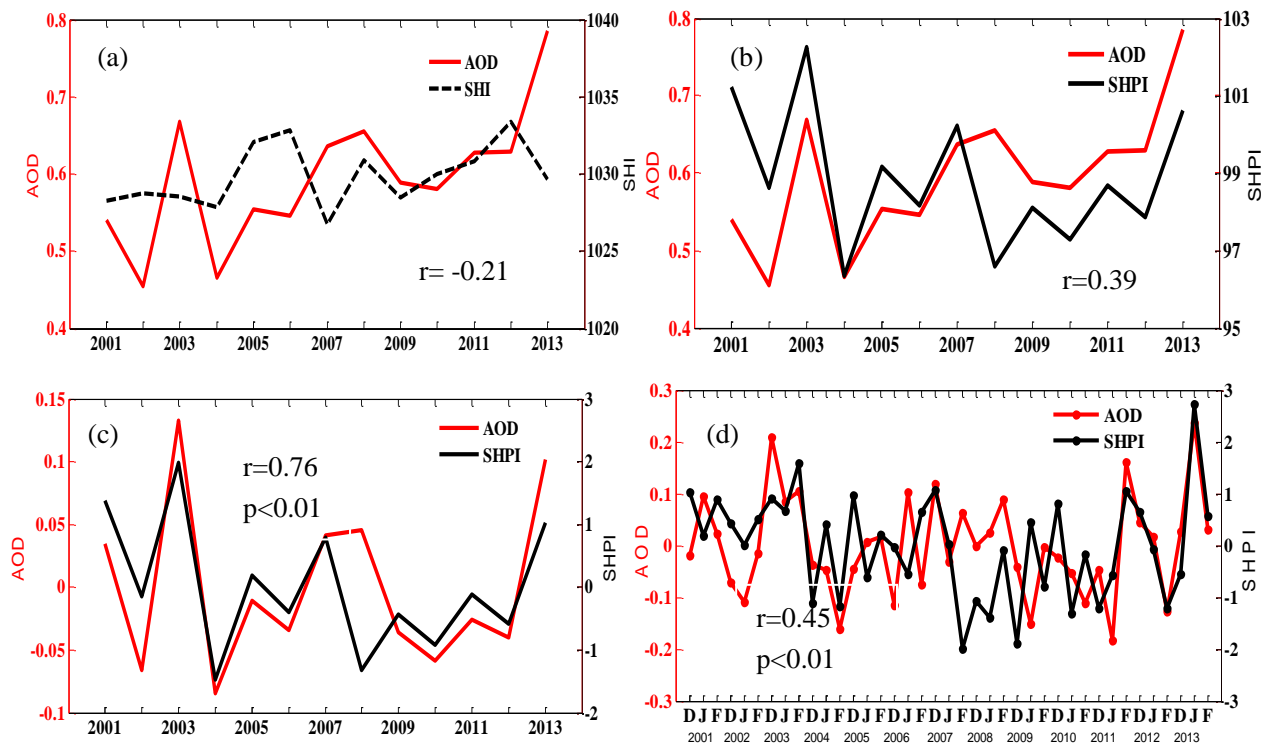
611

612 Figure 4. Difference of SLP (shaded, hPa) and 850 hPa wind vectors (m s^{-1}) between
 613 high- and low-AOD winters; areas with white pluses are differences at the 10%
 614 significance level; the black rectangle outlines the region used in the definition of
 615 conventional SHI. The length of the wind vectors indicates wind speed (m s^{-1}).



616

617 Figure 5. Distribution of winter SLP (shaded) and anomalous (minus 13-year mean)
 618 850 hPa wind fields (vector) in (a) 2003, and (b) 2004; the black solid rectangle
 619 outlines the region used in the definition of SHPI. The length of the wind vectors
 620 indicates wind speed (m s^{-1}).

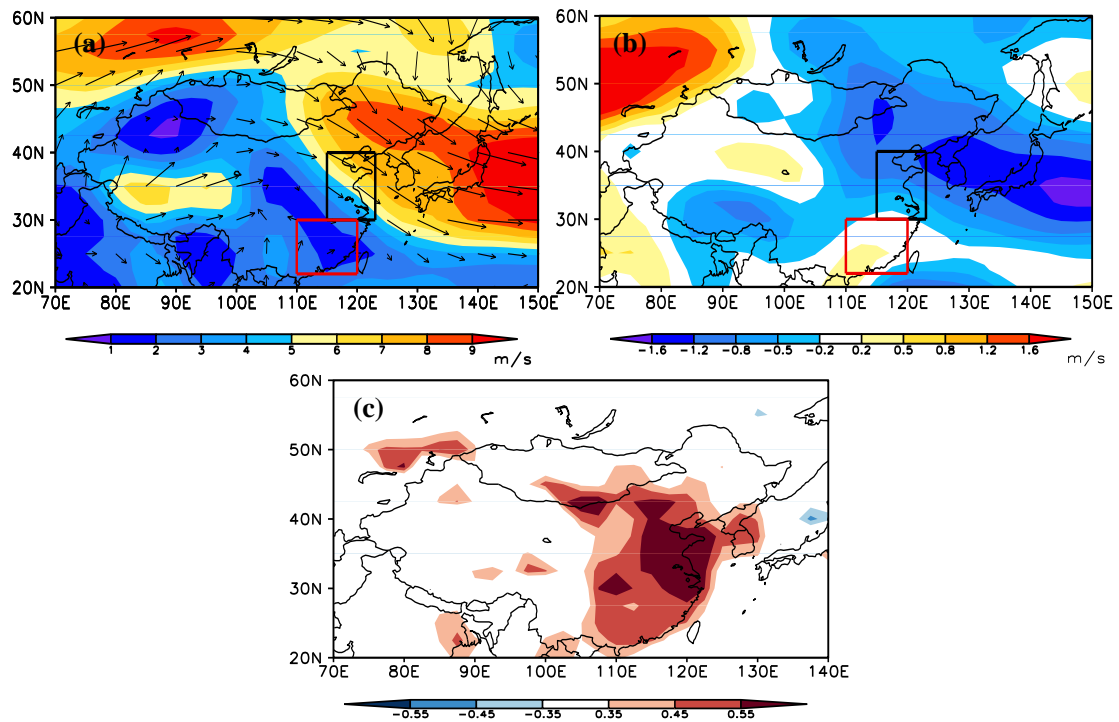


621

622 Figure 6. Time series of wintertime AOD over North China (red lines) with (a) SHI
 623 and (b) SHPI during 2001-2013. (c) Same as (b), but for detrended NC AOD and
 624 normalized SHPI. (d) Detrended NC AOD and normalized SHPI for each winter

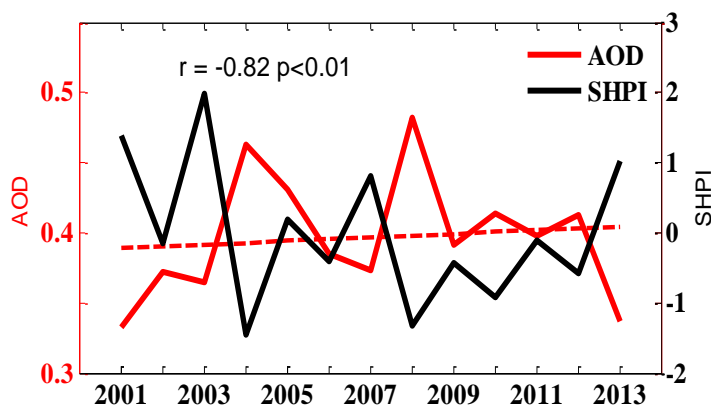
625 month (December, January, February) during 2001-2013.

626



627

628 Figure 7. Geographic distributions of (a) Multi-year (1982-2011) mean winter 850
629 hPa wind direction (vector) and wind speed (shaded), (b) difference of wind speed
630 between high-SHPI year mean and low-SHPI year mean (m s^{-1}), and (c) winter
631 interannual correlation coefficients of SHPI with relative humidity (colored areas are
632 correlations above the 5% significance level).



633

634 Figure 8. Time series of AOD over South China and normalized SHPI.